IEEE Access
Multidisciplinary ⋮ Rapid Review ⋮ Open Access Journal

Received 22 June 2023, accepted 20 July 2023, date of publication 26 July 2023, date of current version 2 August 2023.

Digital Object Identifier 10.1109/ACCESS.2023.3299219

RESEARCH ARTICLE

Energy Detection Based Carrier Sense in LPWAN

SHUSUKE NARIEDA[1], (Member, IEEE), AND TAKEO FUJII[2], (Senior Member, IEEE)
[1]Graduate School of Engineering, Mie University, Tsu, Mie 514-0102, Japan
[2]Advanced Wireless and Communication Research Center (AWCC), The University Electro-Communications, Chofu, Tokyo 182-8585, Japan

Corresponding author: Shusuke Narieda (narieda@pa.info.mie-u.ac.jp)

This research and development work was supported by the Ministry of Internal Affairs and Communications/Strategic Information and Communications R&D Promotion Programme (MIC/SCOPE) #JP215006001.

ABSTRACT Extensive research has been conducted on imperfect carrier sense based on energy detection; however, the effect of the finite packet length, finite carrier sense period, and arbitrary start time of the carrier sense for the arrived signal on the result of the energy detection based carrier sense has never been investigated. This paper presents a detailed discussion on the performances of an energy detection based carrier sense in low-power wide-area network (LPWAN) to detect a target signal with power below the noise power and employ it over a wide communication area. We theoretically derive the finite packet length, finite carrier sense period, and arbitrary start time of the carrier sense as the signal detection deterioration factors. The performance of LPWANs with the energy detection based carrier sense is numerically verified based on these theoretical analyses. The numerical examples demonstrate that the energy detection based carrier sense improves the performance of LPWANs, and an optimum carrier sense level is determined based on the width of the communication area and the packet length on air around the end devices.

INDEX TERMS Carrier sense, energy detection, low-power wide-area networks.

I. INTRODUCTION

The concept of Internet of Things (IoT) is being rapidly adopted in various practical environments. The IoT paradigm relies on a massive IoT devices with wireless transceivers, actuators and physical sensors being deployed to connect and interact between real and virtual worlds. The generated information and values based on knowledge sharing and data analysis can be used to revitalize the industry and solve various social problems. This can be achieved by using wireless sensor networks, and low-power wide-area networks (LPWANs) [1] are one of the technologies employed as the communication infrastructure for the wireless sensor networks in the IoT era.

Low-power wide-area technologies, which operate in the sub-GHz band, can support energy-efficient and long-range communications at the expense of the data rate. Several LPWA technologies have been developed in recent years, such as long range (LoRa) [2], which is based on chirp spread spectrum (CSS) modulation [3], wireless smart utility networks (Wi-SUNs) [4] based on frequency-shift keying (FSK), and SigFox [5] based on differential binary phase-shift keying (DBPSK) and Gaussian FSK. Most of these technologies can be used to construct a private or local network in an unlicensed band. In Japan, LPWA technologies can operate in the sub-GHz band under ARIB STD-T108 regulations [6]. Under these regulations, the end devices perform listen before talk (LBT), that is, carrier sense [7], to coexist with the typical passive tag systems. The end devices without carrier sense can only transmit their data under strictly limited maximum transmission power, maximum transmission time for one packet, and the duty cycle. Furthermore, the end devices with a short carrier sense period of 128 μs are slightly limited by these factors when compared to those with a long carrier sense period of 5 ms. In other regions, such as Europe, the end devices can choose a duty cycle limitation or adaptive frequency agility based on the carrier sense [8], similar to that in Japan.

Carrier sense can be achieved by utilizing signal detection techniques [9], which can be applied to signal processing systems, such as radar systems and digital communication systems. The signal detection problem involves determining the presence of a target signal in the signal, which includes either only noise only or both the target signal and noise; this problem can be considered as a hypothesis testing problem. Several signal detection techniques have been

The associate editor coordinating the review of this manuscript and approving it for publication was Guangjie Han.

developed for various purposes, such as peak power detection, energy detection [10], matched filter based detection [11], and cyclostationary detection [12]. The carrier sense level in ARIB STD-T108 is defined as the instantaneous signal power of one channel at the feed point of the end device, which can be accomplished by using the peak detection. This is the simplest signal detection technique, which involves detecting the maximum power within a given signal detection period; however, noise significantly affects the obtained signal detection results. Therefore, peak detection cannot be used to detect target signals with a power close to the noise power, and is not commonly implemented for a wide communication area. Additionally, CSS based LoRa signals can achieve a high sensitivity below the noise power when compared to other LPWA technologies. For example, the sensitivities of the LoRa signals with spreading factors of 7 and 10 are -123 dBm and -132 dBmm [13], respectively. In contrast, the noise power is approximately -115 dBm for the noise figure at a receiver, and the channel bandwidth is 6 dB and 200 kHz, respectively. Therefore, peak detection cannot effectively detect LoRa signals from other end devices.

The energy detection technique is a simple and powerful signal detection technique that can be used to detect signals, even if the power of the target signal is lower than the noise power. Effective signal detection can be achieved at the end device by utilizing energy detection as the signal detection technique of the carrier sense. However, energy detection is a probabilistic signal detection technique, which causes an imperfect carrier sense that includes miss detection and false alarm probabilities in the hypothesis testing problem. Several analyses have been conducted for carrier sense multiple access (CSMA) under imperfect carrier sense in [14], [15], and [16]. Although miss detection and false alarm are imperfect factors that significantly contribute to errors in signal detection, we have observed that there are more critical factors that affect the performance of LPWAN in energy detection. The theoretical analyses conducted on energy detection assume that the arrived signal length, that is, the packet length, is infinite; however, it is a finite value in the actual environment. Furthermore, carrier sense is not reliably executed from the beginning of the packet. This results in the arrived signal (packet) not occupying the entire carrier sense period. This issue is exacerbated with higher signal detection accuracy, because a low signal detection level requires a long signal detection period. The effect of this issue on the performance of wireless networks has never been investigated in most previous studies. Conversely, the performance of LoRaWAN employing energy detection based LBT and medium access control (MAC) recognition based LBT have been theoretically studied [17]. However, the studies in [17] has not been also discussed the effects of such factors on the performance of LPWAN. Furthermore, although NS-3 based analytical results for CSMA based LoRaWAN [18] and analysis for LoRaWAN with slotted ALOHA and CSMA [19] have been reported, these effects have not been also considered.

This paper presents a detailed discussion on the performance of energy detection based carrier sense in LPWANs. First, the performance of the energy detection based carrier sense is theoretically derived and analyzed. We demonstrate the performance of the energy detection based carrier sense considering several factors under the assumption of an actual carrier sense environment, that is, an arbitrary start time of the carrier sense for the arrived signal, a finite packet length and a finite carrier sense period. Subsequently, the performance of LPWAN with the energy detection based carrier sense is numerically derived based on the derived theoretical analysis results. Assuming actual LPWAN parameters [6], [8], the effects of several factors on the performance of LPWAN are numerically investigated in this study.

The contributions of this study are summarized as follows:

- In this paper, we theoretically derive the performance of the energy detection based carrier sense. Based on the derivation results, we demonstrate the accuracy of the carrier sense results in the deterioration of several factors, that is, the finite packet length, finite carrier sense period and arbitrary start time of the carrier sense for the arrived signal.
- From the above analytical results and the numerical analysis results, we provide that too low the carrier sense level, that is, too long the carrier sense period, deteriorates the performance of LPWAN with the energy detection based carrier sense.
- Considering on the noise power estimation for decision threshold of the energy detection based carrier sense, we carried out the computer simulation. The results show that the effect of interference avoidance by the energy detection based carrier sense outweigh the effect of the degradation of the noise power estimation accuracy owing to interference packets.

The remainder of this paper is organized as follows. In Section II, we define a system model of the carrier sense at the end devices and provide an overview of the characteristics of peak detection and energy detection. The performance of the energy detection based carrier sense is theoretically derived in Section III. Section IV presents the fundamental properties of the energy detection based carrier sense according to the derived results. Section V presents the numerical analysis results of LPWAN with the energy detection based carrier sense. Finally, Section VI presents the conclusions.

II. PRELIMINARY NOTION

A. RECEIVED SIGNAL MODEL AT END DEVICES

First, we employ the received signal model at the end devices. Signal detection of the arrived signal from other end devices can be defined as a binary hypothesis testing problem. We let $\mathcal{H}_0$ and $\mathcal{H}_1$ denote hypotheses that other end devices are inactive or active, respectively, and the complex received signal $r(n)$ with zero mean and variance σ_r^2 is given by,

$$\begin{aligned} \mathcal{H}_1 &: r(n) = w(n) + v(n) \\ \mathcal{H}_0 &: r(n) = v(n), \end{aligned} \tag{1}$$

where $w(n)$ is the complex arrived signal with zero mean and variance σ_w^2, and $w(n) = gs(n)$ where g and $s(n)$ are the channel gain and the transmit signals from other end device and $\sigma_w^2 = g^2\sigma_s^2$. $v(n)$ is an additive white Gaussian noise (AWGN) and $v(n) \sim \mathcal{CN}\left(0, \sigma_v^2/2\right)$ where $\mathcal{CN}(\mathcal{X}, \mathcal{Y})$ is the circularity symmetric complex Gaussian with mean $\mathcal{X}$ and variance $\mathcal{Y}$. We assume that all the signals, that is, $r(n)$, $w(n)$ and $v(n)$ are mutually statistically independent of each other. Furthermore, we assume that the unit of all variances used in this paper is milliwatt, that is, $\sigma_s^2 = 1$ means that the transmit signal power is 1 mW.

B. OVERVIEW OF CHARACTERISTICS FOR PEAK DETECTION

In ARIB STD-T108 [6], which is a communication standard for the sub-GHz band in Japan, the carrier sense level is regulated as simultaneous power at the feed point of the receiver; peak detection can be used to achieve the regulation. We let N and $P_{\mathrm{CS,mW}}$ denote the number of samples corresponding to the signal detection period and carrier sense level, respectively, and the unit of $P_{\mathrm{CS,mW}}$ is in milliwatts. Peak detection is executed as follows:

$$\max_{1\le n\le N} |r(n)|^2 \underset{\mathcal{H}_0}{\overset{\mathcal{H}_1}{\gtrless}} P_{\mathrm{CS,mW}}. \tag{2}$$

Peak detection is a very simple signal detection technique; however, the detection result significantly affects AWGN. Figs. 1 and 2 show the computer simulation results by Matlab for the signal detection and a false alarm probabilities of peak detection, respectively. In Figs. 1 and 2, LoRa signals with $SF = 7$ and $BW = 200\,\mathrm{kHz}$ were employed, and $NF = 6\,\mathrm{dB}$, where $SF \in \{7, 8, 9, 10, 11, 12\}$, BW and NF are spreading factor, channel bandwidth and noise figure of the end devices, respectively. In Fig. 1, the performance of signal detection deteriorated with the decrease in $P_{\mathrm{CS,dBm}}$ where $P_{\mathrm{CS,dBm}} = 10\log_{10}\left(P_{\mathrm{CS,mW}}/1\mathrm{mW}\right)$ is the carrier sense level, and the unit of $P_{\mathrm{CS,dBm}}$ is in decibel milliwatts. Furthermore, the performance of the false alarm probability is drastically deteriorated for $P_{\mathrm{CS,dBm}}$ below approximately $-108\,\mathrm{dBm}$ which is 9 dB larger than the noise power, which is given by [20]

$$\eta_{\mathrm{dBm}} = -174 + 10\log_{10}(BW) + NF. \tag{3}$$

Note that the noise power η_{dBm} is given by $\eta_{\mathrm{dBm}} \approx -115\,\mathrm{dBm}$ for the parameters, BW and NF, defined earlier. This is because the peak detection results significantly affects AWGN, and it can be seen that the peak detection based carrier sense cannot achieve low carrier sense levels near and below the noise power.

C. ENERGY DETECTION

The energy detection technique is based on the average energy of the received signals in a fixed period, and a statistic

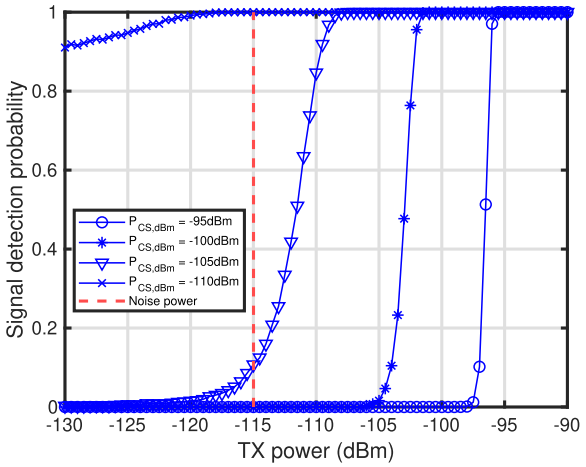

FIGURE 1. Signal detection probability of peak detection.

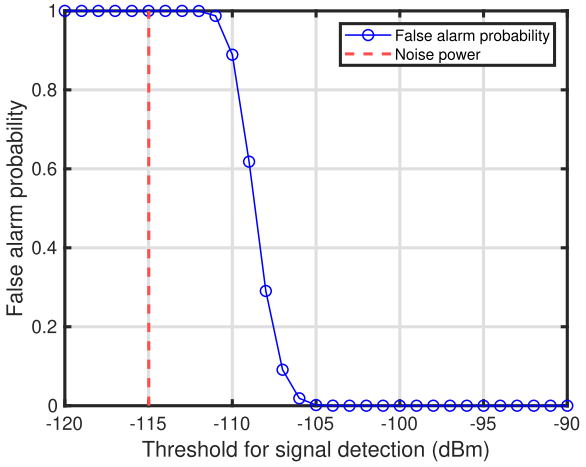

FIGURE 2. False alarm probability of peak detection.

for energy detection S_r can be written as,

$$S_r = \frac{1}{N}\sum_{n=0}^{N-1} |r(n)|^2, \tag{4}$$

where N is the number of samples used for signal detection. S_r is considered a probabilistic variable. S_r follows a Chi-square distribution with $2N$ degrees of freedom, which can be approximated as $\mathcal{CN}\left(\widetilde{\mu}_r, \widetilde{\sigma}_r^2\right)$ for a sufficiently large N, that is, the central limit theorem [21] can be achieved, where $\mathcal{CN}(\mathcal{X}, \mathcal{Y})$, $\widetilde{\mu}_r$, and $\widetilde{\sigma}_r^2$ are the circularity symmetric complex Gaussian with mean $\mathcal{X}$ and variance $\mathcal{Y}$, the mean of S_r, and the variance of S_r, respectively. Furthermore, $\widetilde{\mu}_r = \sigma_r^2$ and $\widetilde{\sigma}_r^2 = \sigma_r^4/N$. The probability density function of S_r is given by,

$$p_{S_r}(x) = \frac{1}{\sqrt{2\pi\widetilde{\sigma}_r^2}} \exp\left\{-\frac{(x-\widetilde{\mu}_r)^2}{2\widetilde{\sigma}_r^2}\right\}. \tag{5}$$

The signal detection result can be obtained by comparing S_r with the carrier sense level $P_{\mathrm{CS,mW}}$, as follows,

$$S_r \underset{\mathcal{H}_0}{\overset{\mathcal{H}_1}{\gtrless}} P_{\mathrm{CS,mW}}. \tag{6}$$

On the other hand, a statistic S_v when the target signal is inactive is given by,

$$S_v = \frac{1}{N}\sum_{n=0}^{N-1} |v(n)|^2 . \tag{7}$$

Similar to S_r, S_v follows $\mathcal{CN}\left(\sigma_v^2, \sigma_v^4/N\right)$ for a sufficiently large N, and the probability density function of S_v can be written as

$$p_{S_v}(x) = \frac{1}{\sqrt{2\pi\sigma_v^4/N}} \exp\left\{-\frac{\left(x-\sigma_v^2\right)^2}{2\sigma_v^4/N}\right\}. \tag{8}$$

From eq. (8), the target false alarm probability $\overline{P_{\mathrm{FA}}}$ is given by

$$\overline{P_{\mathrm{FA}}} = Q\left\{\left(\frac{P_{\mathrm{CS,mW}}}{\sigma_v^2} - 1\right)\sqrt{N}\right\}, \tag{9}$$

where $Q(\mathcal{X}) = \frac{1}{\sqrt{2}}\int_{\mathcal{X}}^{\infty} e^{-t^2/2}dt$ [22], and $P_{\mathrm{CS,mW}}$ can be written as

$$P_{\mathrm{CS,mW}} = \sigma_v^2\left\{\frac{Q^{-1}\left(\overline{P_{\mathrm{FA}}}\right)}{\sqrt{N}} + 1\right\}, \tag{10}$$

where $Q^{-1}(\cdot)$ is the inverse function of $Q(\cdot)$. Based on $P_{\mathrm{CS,mW}}$, the signal detection probability is given by

$$\begin{aligned} P_{\mathrm{D}} &= \int_{P_{\mathrm{CS,mW}}}^{\infty} p_r(x)dx \\ &= Q\left[\frac{1}{1+\gamma}\left\{Q^{-1}\left(\overline{P_{\mathrm{FA}}}\right) - \gamma\sqrt{N}\right\}\right], \end{aligned} \tag{11}$$

where $\gamma = \sigma_w^2/\sigma_v^2$. We let T denote the period for signal detection, and eq. (11) can be also written as

$$P_{\mathrm{D}} = Q\left[\frac{1}{1+\gamma}\left\{Q^{-1}\left(\overline{P_{\mathrm{FA}}}\right) - \gamma\sqrt{\frac{T}{2BW}}\right\}\right]. \tag{12}$$

Furthermore, the following equations can be obtained,

$$N = \frac{T}{2BW} = \frac{1}{\gamma^2}\left\{Q^{-1}\left(\overline{P_{\mathrm{FA}}}\right) - (1+\gamma)\,Q^{-1}\left(\overline{P_{\mathrm{D}}}\right)\right\}^2, \tag{13}$$

where $\overline{P_{\mathrm{D}}}$ is the target signal detection probability. Furthermore, eq. (13) also indicates the number of samples required to satisfy the carrier sense level $P_{\mathrm{CS,mW}}$ by substituting the SNR γ in eq. (13) with $P_{\mathrm{CS,mW}}/\sigma_v^2$.

Energy detection can achieve lower signal detection levels compared to peak detection. The signal detection level of energy detection is fundamentally determined by the signal detection period and the target false alarm probability as shown in this subsection. In addition, the accuracy of noise power estimation at the receiver determines the signal detection level, and the inaccurate estimation results in SNR wall phenomenon [23]. The inaccurate noise power estimation is caused by four factors, that is, temperature variation, change in low noise amplifier gain owing to thermal fluctuations, initial calibration error and presence of interferes [24]. Note that the first three factors are caused by thermal changes. It is well known that the problem caused by thermal changes can be almost overcome by the noise power estimation with a sufficient period because thermal changes are very slow [25]. The effect of these factors on the performance of LPWAN, especially the effect of the last one on the LPWAN, is discussed based on computer simulation results at the later section.

III. CHARACTERISTICS OF CARRIER SENSE BASED ON ENERGY DETECTION

A. OVERVIEW

In this section, we theoretically derive the characteristics of the energy detection based carrier sense. By employing energy detection to the carrier sense, it can be expected the carrier sense that can detect the target signals with the power below noise power. However, to further lower the carrier sense level, the carrier sense period T_{CS} must be extended. Note that T_{CS} can be obtained from eq. (13) with T replaced by T_{CS}. Fig. 3 depicts the relationship between the carrier sense level and the carrier sense period obtained from eq. (13). In Fig. 3, $\overline{P_{\mathrm{D}}} = 0.99$ and $\overline{P_{\mathrm{FA}}} = 10^{-4}$ were employed as the parameter for signal detection, and $NF = 6\,\mathrm{dB}$, $BW = 200\,\mathrm{kHz}$, and LoRa signals with $SF = 7$ were assumed. The carrier sense periods $T_{\mathrm{CS}} = 1\,\mathrm{ms}$, $10\,\mathrm{ms}$, and $100\,\mathrm{ms}$ are required to achieve the carrier sense level $P_{\mathrm{CS,dBm}} = -120\,\mathrm{dBm}$, $-125\,\mathrm{dBm}$, and $-130\,\mathrm{dBm}$, respectively. It can be seen that the required carrier sense period increases by 10 times as the carrier sense level decreases by 5 dB.

We let T_{TOA} denote the time on air of a packet, that is, the arrived signal length of a packet. The theoretical analyses of energy detection presented in the previous section assume that the arrived signals occupy the entire carrier sense period, that is, $T_{\mathrm{TOA}}/T_{\mathrm{CS}}$ approximates infinity. Fig. 4 illustrates the relationship between $T_{\mathrm{TOA}}/T_{\mathrm{CS}}$ and T_{TOA}. Note that T_{CS} can be obtained using eq. (13) where γ is substituted by $P_{\mathrm{CS,mW}}/\sigma_v^2$. In Fig. 4, LoRa signals with $SF = 7$, 10, and 12 are considered, and the payload lengths are 6 byte; the T_{TOA} for each LoRa signal is 61.7 ms, 370.7 ms, and 1318.9 ms, respectively. The ratio $T_{\mathrm{TOA}}/T_{\mathrm{CS}}$ decreases with the decrease in the carrier sense level, and the ratios for the LoRa signals with $SF = 7$, 10, and 12 are below 10 for $P_{\mathrm{CS,dBm}} = -124\,\mathrm{dBm}$, $-128\,\mathrm{dBm}$, and $-131\,\mathrm{dBm}$, respectively. Consequently, $T_{\mathrm{TOA}}/T_{\mathrm{CS}}$ cannot be approximated as infinity, and $T_{\mathrm{TOA}}/T_{\mathrm{CS}}$ must be considered as a finite value, as demonstrated above. Furthermore, the beginning of the arrived signals may not be accurately captured by the carrier sense. This results in the carrier sense period to not be fully occupied by the arrived signal, that is, the carrier sense can occur with insufficient arrived signal length. Therefore, the

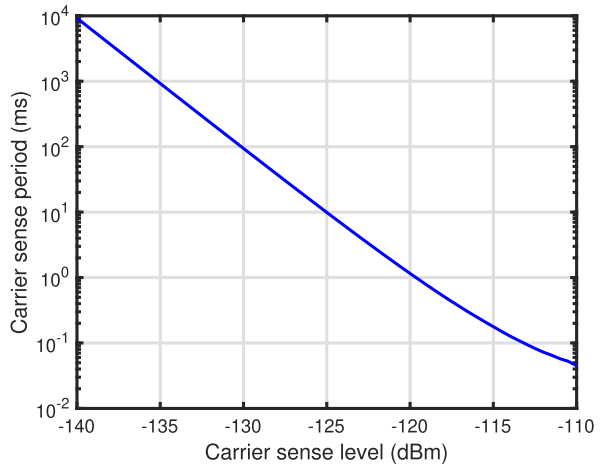

FIGURE 3. Relationship between carrier sense level and carrier sense period.

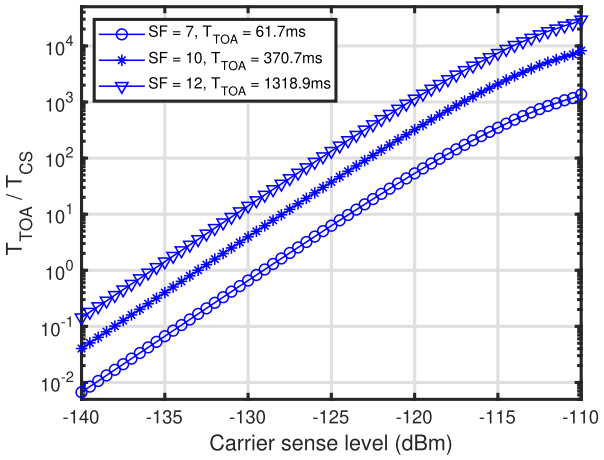

FIGURE 4. Relationship between carrier sense level and $T_{\mathrm{TOA}}/T_{\mathrm{CS}}$.

characteristics of the energy detection based carrier sense vary from those of energy detection.

Based on the findings, in this section, we provide the theoretical analyses of signal detection probability, that is, carrier sense success probability. By deriving the probability for given the carrier sense period T_{CS} and the length of arrived packet T_{TOA}, we investigate the capability of energy detection based carrier sense in LPWAN. To obtain this, we first derive the characteristics of carrier sense with insufficient signal length, that is, $N_{\mathrm{CS}} \geq N_{\mathrm{TOA}}$ where N_{CS} and N_{TOA} are the number of samples for the carrier sense and the number of samples for the arrived signal, respectively. Furthermore, $N_{\mathrm{CS}} = T_{\mathrm{CS}}/2BW$ and $N_{\mathrm{TOA}} = T_{\mathrm{TOA}}/2BW$. Next, we derive the characteristics considering on the arbitrariness of the carrier sense start time for the arrived signal.

B. SIGNAL DETECTION PROBABILITY; ARRIVED SIGNAL LENGTH LOWER THAN CARRIER SENSE PERIOD

The theoretical values for $N_{\mathrm{CS}} \geq N_{\mathrm{TOA}}$ are derived in this subsection. Considering on the finite length of the packet and the finite length of the carrier sense period, $r(n)$ shown in eq. (1) can be rewritten as,

$$\mathcal{H}_1 : r(n) = \begin{cases} w(n) + v(n), & K \leq n \leq K + N_{\mathrm{TOA}} - 1 \\ v(n), & 0 \leq n \leq K - 1, \\ & K + N_{\mathrm{TOA}} \leq N_{\mathrm{CS}} - 1 \end{cases} \tag{14}$$

$$\mathcal{H}_0 : r(n) = v(n),\ 0 \leq n \leq N_{\mathrm{CS}} - 1 \tag{15}$$

where K is an arbitrary positive number and $0 \leq K \leq N_{\mathrm{CS}} - N_{\mathrm{TOA}}$. Since only $v(n)$ occupies the carrier sense period regardless of the arrived signal length, the statistic $S_{\mathrm{CS},v}$ for the case, where the other end devices are inactive, is given by

$$S_{\mathrm{CS},v} = \frac{1}{N_{\mathrm{CS}}} \sum_{n=0}^{N_{\mathrm{CS}}-1} |v(n)|^2 . \tag{16}$$

The statistical property of $S_{\mathrm{CS},v}$ is essentially the identical to that of T_v, and signal detection in the carrier sense is executed by comparing a statistic with the threshold $P_{\mathrm{CS,mW}}$. The statistic $S_{\mathrm{CS},r}$, where the other end devices are active, can be written as

$$\begin{aligned} S_{\mathrm{CS},r} &= \frac{1}{N_{\mathrm{CS}}} \sum_{n=0}^{N_{\mathrm{CS}}-1} |r(n)|^2 \\ &= \frac{1}{N_{\mathrm{CS}}} \left\{ \sum_{n=0}^{K-1} |v(n)|^2 + \sum_{n=K}^{K+N_{\mathrm{TOA}}-1} |w(n) + v(n)|^2 \right. \\ &\quad \left. + \sum_{n=K+N_{\mathrm{TOA}}}^{N-1} |v(n)|^2 \right\} \\ &\approx \frac{1}{N_{\mathrm{CS}}} \left\{ K\sigma_v^2 + N_{\mathrm{TOA}} \left(\sigma_w^2 + \sigma_v^2 \right) \right. \\ &\quad \left. + (N_{\mathrm{CS}} - K - N_{\mathrm{TOA}})\, \sigma_v^2 \right\} \\ &= \sigma_v^2 + \frac{N_{\mathrm{TOA}}}{N_{\mathrm{CS}}} \sigma_w^2 . \end{aligned} \tag{17}$$

Signal detection in the carrier sense is achieved by comparing $S_{\mathrm{CS},r}$ with the threshold $P_{\mathrm{CS,mW}}$. Assuming a sufficiently large N_{TOA}, $S_{\mathrm{CS},r}$ follows the probability density function $p_{\mathrm{CS},r}(x)$ as shown in the following equations,

$$\begin{aligned} p_{\mathrm{CS},r}(x) = & \frac{1}{\sqrt{\frac{2\pi \left(\sigma_v^2 + \frac{N_{\mathrm{TOA}}}{N_{\mathrm{CS}}} \sigma_w^2 \right)^2}{N_{\mathrm{CS}}}}} \\ & \cdot \exp \left\{ - \frac{\left(x - \sigma_v^2 - \frac{N_{\mathrm{TOA}}}{N_{\mathrm{CS}}} \sigma_w^2 \right)^2}{\frac{2 \left(\sigma_v^2 + \frac{N_{\mathrm{TOA}}}{N_{\mathrm{CS}}} \sigma_w^2 \right)^2}{N_{\mathrm{CS}}}} \right\} . \end{aligned} \tag{18}$$

The signal detection probability $P_{\mathrm{D,CS}}$ can be derived as,

$$\begin{aligned} P_{\mathrm{D,CS}} &= \int_{P_{\mathrm{CS,mW}}}^{\infty} p_{\mathrm{CS},r}(x) dx \\ &= Q \left\{ \left(\frac{P_{\mathrm{CS,mW}}}{\sigma_v^2 + \frac{N_{\mathrm{TOA}}}{N_{\mathrm{CS}}} \sigma_w^2} - 1 \right) \sqrt{N_{\mathrm{CS}}} \right\} . \end{aligned} \tag{19}$$

We let $\overline{P_{\mathrm{D,CS}}}(N_{\mathrm{TOA}})$ denote an extended version of $P_{\mathrm{D,CS}}$ for arbitrary K and N_{TOA}. Then, $\overline{P_{\mathrm{D,CS}}}(N_{\mathrm{TOA}})$ can be derived as,

$$\overline{P_{\mathrm{D,CS}}}(N_{\mathrm{TOA}}) = Q\left\{\left(\frac{P_{\mathrm{CS,mW}}}{\sigma_v^2+\min\left(1,\frac{N_{\mathrm{TOA}}}{N_{\mathrm{CS}}}\right)\sigma_w^2}-1\right)\sqrt{N_{\mathrm{CS}}}\right\}, \quad (20)$$

where $\min(\mathcal{X},\mathcal{Y})$ is a function which returns the minimum value between $\mathcal{X}$ and $\mathcal{Y}$. Furthermore, eq. (20) can also be defined as a function of T_{TOA},

$$\overline{P_{\mathrm{D,CS}}}(T_{\mathrm{TOA}}) = Q\left\{\left(\frac{P_{\mathrm{CS,mW}}}{\sigma_v^2+\min\left(1,\frac{T_{\mathrm{TOA}}}{T_{\mathrm{CS}}}\right)\sigma_w^2}-1\right)\sqrt{\frac{T_{\mathrm{CS}}}{2BW}}\right\}. \quad (21)$$

C. SIGNAL DETECTION PROBABILITY: ARBITRARY START TIME OF CARRIER SENSE FOR ARRIVED SIGNAL

We assume that the start time of the carrier sense for the arrived signals follows an uniform distribution, and the signal detection probability is determined in two cases. In the first case, the carrier sense period is less than the arrived signal length, that is, $N_{\mathrm{TOA}} \geq N_{\mathrm{CS}}$. In the second case, the carrier sense period is longer than the arrived signal length, that is, $N_{\mathrm{TOA}} < N_{\mathrm{CS}}$. Considering that the start time of the carrier sense is arbitrary, the two cases, i.e., the case where the arrived signal occupies either all or a part of the carrier sense period, must be discussed. We discuss the first case as shown in Fig. 5(1). The number of samples available for the carrier sense varies from 1 to $N_{\mathrm{CS}}-1$ for the upper two signals in Fig. 5(1), and the number of samples available for the carrier sense varies from $N_{\mathrm{CS}}-1$ to 1 for the lower two signals in Fig. 5(1). Based on $\overline{P_{\mathrm{D,CS}}}(N_{\mathrm{TOA}})$, the sum of the signal detection probabilities at each position of the arrived signal $P_{\mathrm{CS1},1}$ is given by,

$$P_{\mathrm{CS1},1} = 2\sum_{n=1}^{N_{\mathrm{CS}}-1}\overline{P_{\mathrm{D,CS}}}(n). \quad (22)$$

Subsequently, we discuss the case illustrated in Fig. 5(2). Note that the signal detection probability in this case is identical to that in the general case, as shown in eq. (11). We let $P_{\mathrm{CS1},2}$ denote the sum of the signal detection probability at each position of the arrived signal, which can be written as

$$P_{\mathrm{CS1},2} = (N_{\mathrm{TOA}}-N_{\mathrm{CS}}+1)\,\overline{P_{\mathrm{D,CS}}}(N_{\mathrm{CS}}). \quad (23)$$

The signal detection probability P_{CS1} for $N_{\mathrm{TOA}} \geq N_{\mathrm{CS}}$ can be obtained by taking the average of $P_{\mathrm{CS1},1}$ and $P_{\mathrm{CS1},2}$ as follows,

$$\begin{aligned}P_{\mathrm{CS1}} &= \frac{P_{\mathrm{CS1},1}+P_{\mathrm{CS1},2}}{N_{\mathrm{CS}}+N_{\mathrm{TOA}}}\\ &= \frac{1}{N_{\mathrm{CS}}+N_{\mathrm{TOA}}}\cdot\left\{2\sum_{n=1}^{N_{\mathrm{CS}}-1}\overline{P_{\mathrm{D,CS}}}(n)\right.\\ &\quad\left.+(N_{\mathrm{TOA}}-N_{\mathrm{CS}}+1)\,\overline{P_{\mathrm{D,CS}}}(N_{\mathrm{CS}})\right\}. \quad (24)\end{aligned}$$

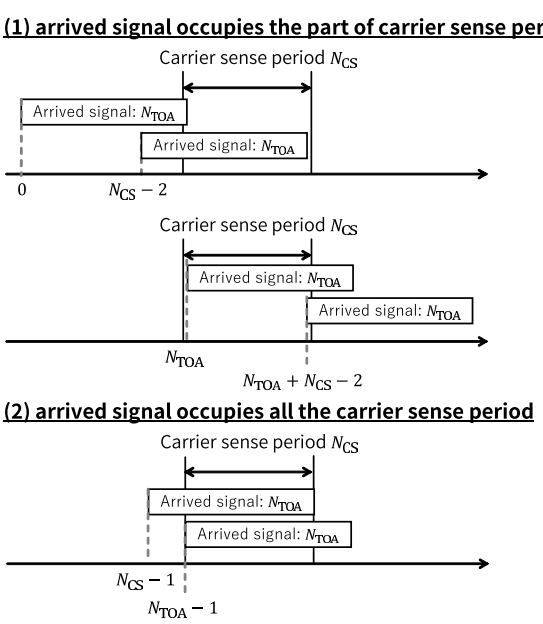

FIGURE 5. $N_{\mathrm{TOA}} \geq N_{\mathrm{CS}}$ case where carrier sense period is longer than arrived signal length.

Here, we discuss the case in which the carrier sense period is longer than the arrived signal length, that is, $N_{\mathrm{TOA}} < N_{\mathrm{CS}}$. First, we discuss the case in which a part of the arrived signals is included within the carrier sense period, as shown in Fig. 6(1). Similar to eq. (22), the sum of the signal detection probabilities $P_{\mathrm{CS2},1}$ at each position of arrived signals is given by

$$P_{\mathrm{CS2},1} = 2\sum_{n=1}^{N_{\mathrm{TOA}}-1}\overline{P_{\mathrm{D,CS}}}(n). \quad (25)$$

For the case in which all the arrived signals are included within the carrier sense period, as shown in Fig. 6, the sum of the signal detection probabilities at each position of the arrived signals can be written as

$$P_{\mathrm{CS2},2} = (N_{\mathrm{CS}}-N_{\mathrm{TOA}}+1)\,\overline{P_{\mathrm{D,CS}}}(N_{\mathrm{TOA}}). \quad (26)$$

From these, the signal detection probability P_{CS2} for $N_{\mathrm{TOA}} < N_{\mathrm{CS}}$ can be obtained by taking the average of $P_{\mathrm{CS2},1}$ and $P_{\mathrm{CS2},2}$ as

$$\begin{aligned}P_{\mathrm{CS2}} &= \frac{P_{\mathrm{CS2},1}+P_{\mathrm{CS2},2}}{N_{\mathrm{CS}}+N_{\mathrm{TOA}}}\\ &= \frac{1}{N_{\mathrm{CS}}+N_{\mathrm{TOA}}}\cdot\left\{2\sum_{n=1}^{N_{\mathrm{TOA}}-1}\overline{P_{\mathrm{D,CS}}}(n)\right.\\ &\quad\left.+(N_{\mathrm{CS}}-N_{\mathrm{TOA}}+1)\,\overline{P_{\mathrm{D,CS}}}(N_{\mathrm{TOA}})\right\}. \quad (27)\end{aligned}$$

The carrier sense success probability P_{CS} can be represented using eqs. (24) and (27) as follows,

$$P_{\mathrm{CS}} = \begin{cases}P_{\mathrm{CS1}}, & N_{\mathrm{TOA}} \geq N_{\mathrm{CS}}\\ P_{\mathrm{CS2}}, & N_{\mathrm{TOA}} < N_{\mathrm{CS}}\end{cases}. \quad (28)$$

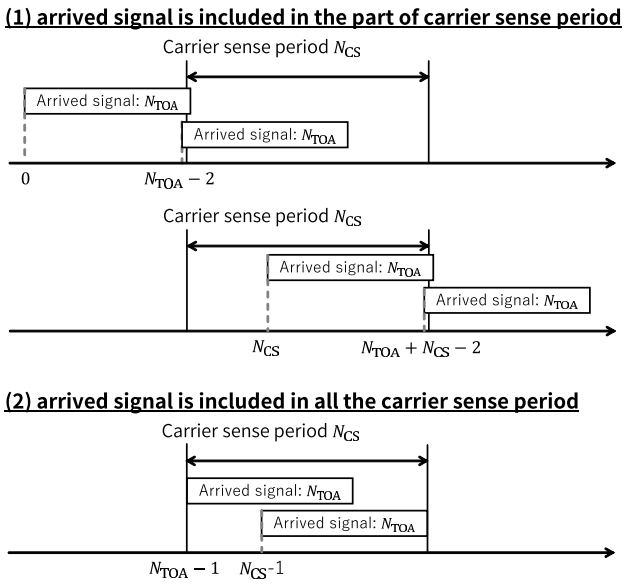

FIGURE 6. $N_{TOA} < N_{CS}$ case where carrier sense period is less than arrived signal length.

IV. FUNDAMENTAL PROPERTIES OF ENERGY DETECTION BASED CARRIER SENSE

A. OVERVIEW

In this subsection, we present some fundamental properties of the energy detection based carrier sense based on the derivation results obtained in the previous subsection. First, the properties of the energy detection based carrier sense are presented as a signal detection scheme. Subsequently, the properties of the actual LPWAN environments are provided assuming the actual LPWAN parameters. The theoretical and numerical examples shown in this section were obtained under $\overline{P_D} = 0.99$, $\overline{P_{FA}} = 10^{-4}$, $BW = 200\,\text{kHz}$, and $NF = 6\,\text{dB}$.

B. SIGNAL DETECTION PROBABILITIES FOR $N_{TOA} < N_{CS}$

In this subsection, we present the theoretical and numerical examples of signal detection probabilities for $N_{TOA} < N_{CS}$. All the results presented in this subsection assume that all the arrived signals are included within the carrier sense period in order to focus on the properties for $N_{TOA} < N_{CS}$. Fig. 7 illustrates the signal detection probabilities for $N_{TOA} < N_{CS}$, that is, it is depicted that the carrier sense period is longer than the arrived signal length. Fig. 7 presents a comparison of the theoretical and numerical values for $N_{CS} = 2048$ and $N_{TOA} = 256$, 512, and 1024. The derived theoretical and numerical values concur well with each other, and the performance of the signal detection probability deteriorates with the decrease in the arrived signal length N_{TOA}. Fig. 8 depicts the comparison results of the signal detection probabilities for $N_{TOA} < N_{CS}$ and $N_{TOA} = N_{CS}$ for $N = 2048$ and $N_{TOA} = 256$, 512, and 1024. The performance of the signal detection probabilities for $N_{TOA} < N_{CS}$ is inferior to that for $N_{TOA} = N_{CS}$ with the decrease in N_{TOA}/N_{CS}, as shown in Fig. 8.

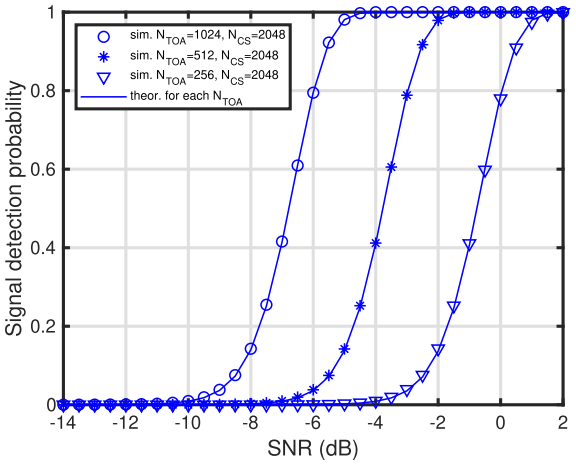

FIGURE 7. Theoretical and numerical results of signal detection probability for $N_{TOA} < N_{CS}$.

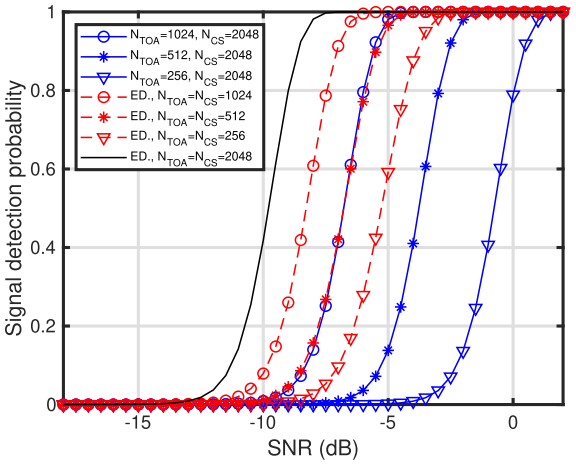

FIGURE 8. Comparison results of theoretical signal detection probability between $N_{TOA} < N_{CS}$ case and $N_{TOA} = N_{CS}$ case.

C. SIGNAL DETECTION PROBABILITIES CONSIDERING ARBITRARY START TIME OF CARRIER SENSE

In this subsection, we present the theoretical and numerical examples of the signal detection probabilities in which the carrier sense begins at an arbitrary time for the arrived signals. Especially, the following two properties are discussed in this subsection: the ratio N_{TOA}/N_{CS} is varied under a fixed N_{CS}, and the ratio N_{TOA}/N_{CS} is varied under a fixed N_{TOA}.

We demonstrate the theoretical and numerical performances of the signal detection probabilities considering the arbitrary carrier sense start time. Fig. 9 presents the comparison results of the theoretical performances, which are obtained from eq (28), and the numerical performances for $N_{CS} = 4096$, $N_{TOA} = 65536$, 16384, 4096, 1024, 256 ($N_{TOA}/N_{CS} = 16, 4, 1, 0.25, 0.625$). We first demonstrate the characteristic under a fixed carrier sense period N for

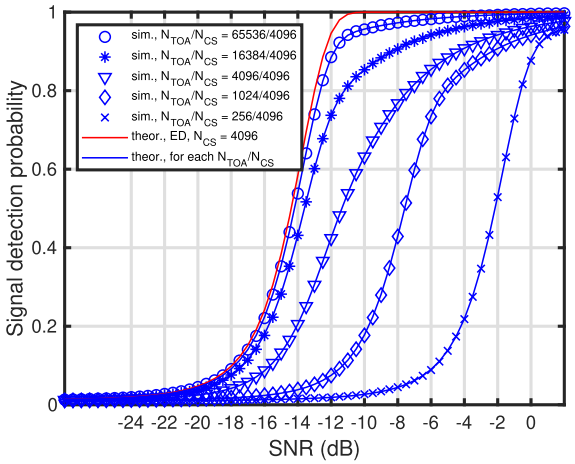

FIGURE 9. Theoretical and numerical results of signal detection probability considering an arbitrary carrier sense start time.

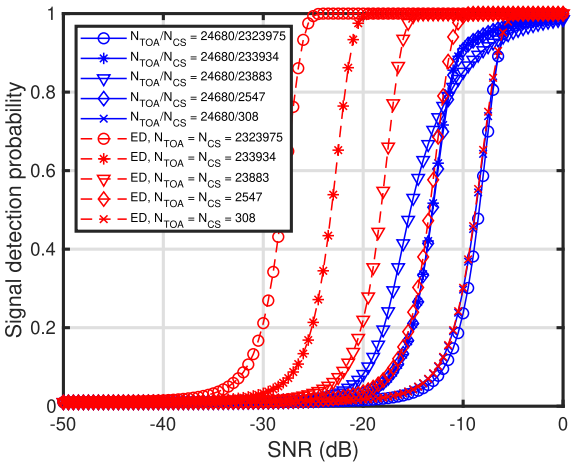

FIGURE 10. Comparison results of signal detection probability between $N_{TOA} > N_{CS}$ case and $N_{TOA} = N_{CS}$ case. $N_{TOA} = 24680$ and $N_{CS} = 2323975, 233934, 23883, 2547, 308$ ($N_{TOA}/N_{CS} = 0.01, 0.11, 1.03, 9.69, 80.13$).

different arrived signal lengths N_{TOA}. The derived theoretical and numerical values concur well. The performance for a large $N_{\mathrm{TOA}}/N_{\mathrm{CS}}$ is observed to be almost identical that of the energy detection technique ($N_{\mathrm{CS}} = 4096$); however, the performance deteriorates with the decrease in $N_{\mathrm{TOA}}/N_{\mathrm{CS}}$. This is attributed to the increase in the probability that the arrived signal occupies the carrier sense period. Furthermore, for two curves with the same $N_{\mathrm{TOA}}/N_{\mathrm{CS}}$ and its reciprocal, for example, $N_{\mathrm{TOA}}/N_{\mathrm{CS}} = 16$ and $N_{\mathrm{TOA}}/N_{\mathrm{CS}} = 0.0625$, the form of the two curves themselves, that is, the gentle of the two curves, is almost identical. The gradient approximates the theoretical value obtained from eq. (11) as $N_{\mathrm{TOA}}/N_{\mathrm{CS}}$ or $N_{\mathrm{CS}}/N_{\mathrm{TOA}}$ approaches ∞. Furthermore, the gradient becomes gentle as $N_{\mathrm{TOA}}/N_{\mathrm{CS}}$ or $N_{\mathrm{CS}}/N_{\mathrm{TOA}}$ approaches 1. This can be explained as follows. In the case where $N_{\mathrm{TOA}}/N_{\mathrm{CS}}$ is sufficiently large, all the carrier sense periods are likely to be occupied by the arrived signals, and therefore, the gradient of the curves approximates the curves given by eq. (11). In the case where $N_{\mathrm{CS}}/N_{\mathrm{TOA}}$ is sufficiently large, all the arrived signals are likely to be included within the carrier sense period. Consequently, the gradient of the curves also approximates the curves given by eq. (11), as shown in Fig. 8. Conversely, in the case where $N_{\mathrm{TOA}}/N_{\mathrm{CS}} \approx 1$, all the carrier sense periods are not likely to be occupied by the arrived signals; essentially, the arrived signals are not likely to be included within the carrier sense period. This produces an insufficient number of samples for signal detection resulting in a gentle gradient of the curves, which is described by eqs. (24) and (27). The analysis of the gentle of the curves is crucial in determining the characteristics of the energy detection based carrier sense, which are presented in the next subsection.

Subsequently, we present the characteristics under a fixed arrived signal length N_{TOA} for different carrier sense periods N_{CS}. Fig. 10 presents the comparison result of the signal detection probability for $N_{\mathrm{TOA}} = 24680$ and $N_{\mathrm{CS}} = 2323975, 233934, 23883, 2547, 308$ ($N_{\mathrm{TOA}}/N_{\mathrm{CS}} = 0.01, 0.11, 1.03, 9.69, 80.13$). The theoretical values based on eq. (28) and the theoretical values for energy detection shown in eq. (11) are compared. The performance of the probability considering the arbitrary carrier sense start time deteriorates with the decrease in $N_{\mathrm{TOA}}/N_{\mathrm{CS}}$. As $N_{\mathrm{TOA}}/N_{\mathrm{CS}}$ increases, the performance approaches that shown in eq. (11); the performance deteriorates because the carrier sense period N_{CS} decreases. Fig. 11 presents the comparison result of the signal detection probability focusing on Fig. 11 to present the details for the characteristic of the derived theoretical values. Fig. 11 shows that the performances deteriorate in the order of $N_{\mathrm{CS}} = 2323975, 233934, 23883$, and the performances improve as $N_{\mathrm{CS}} = 2547, 308$. By arranging these performances in descending order, it can be seen that the order is the same as the order arranged in descending order of the gradient of the curves in Fig. (9). Similar to the analysis presented in Fig. 10, the analysis is also important for revealing the characteristics of the energy detection based carrier sense.

D. SIGNAL DETECTION PROBABILITIES FOR DIFFERENT CARRIER SENSE LEVELS

Based on the analytical results obtained in the previous subsection, we present numerical examples for the actual LPWAN parameters. Fig. 12 depicts the signal detection probability for different carrier sense levels. In Fig. 12, the arrived signal is assumed to be a LoRa signal with $SF = 7$ and payload length 6 byte, that is, $T_{\mathrm{TOA}} = 61.7$ ms, and the theoretical performances are shown for the received signal powers of the arrived signals of -119 dBm, -121.5 dBm and -124 dBm. It can be seen that the performance deteriorates at the carrier sense level far from the center $P_{\mathrm{CS,dBm}} = -129$ dBm, for all results in Fig. 12. This is because good performance cannot be obtained for a carrier sense period which is either too long or too short, as observed from the results obtained in the previous subsection. Furthermore,

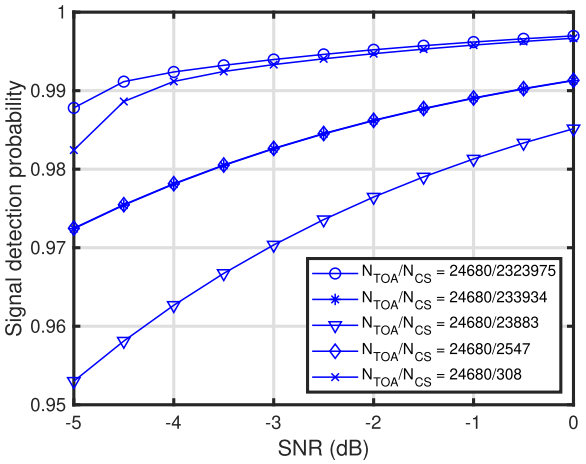

FIGURE 11. Signal detection probability. $N_{TOA} = 24680$ and $N_{CS} = 2323975, 233934, 23883, 2547, 308$ ($N_{TOA}/N_{CS} = 0.01, 0.11, 1.03, 9.69, 80.13$).

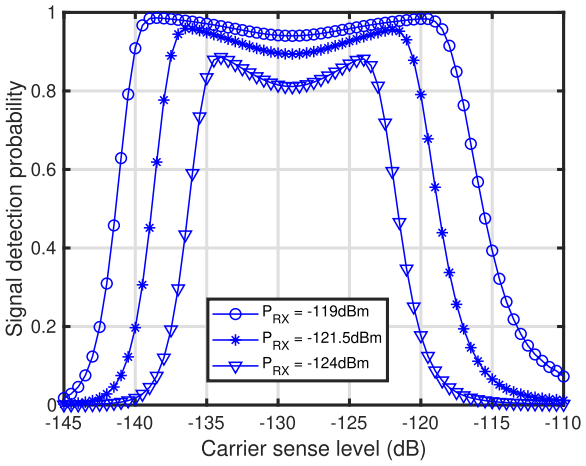

FIGURE 12. Signal detection probability for different $P_{CS,dBm}$. $P_{RX} = -119$ dBm, -121.5 dBm, -124 dBm and $T_{TOA} = 61.7$ ms.

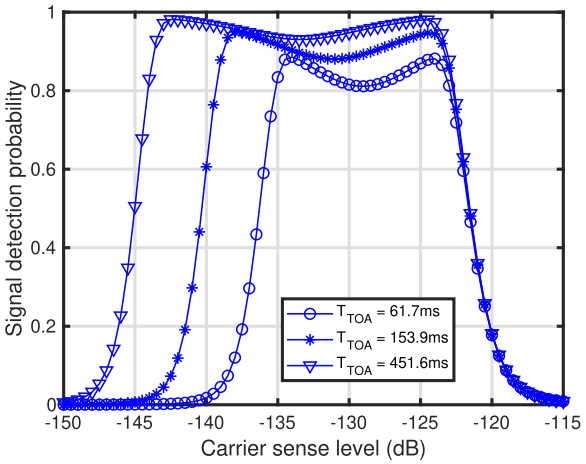

FIGURE 13. Signal detection probability for different $P_{CS,dBm}$. $P_{RX} = -124$ dBm, $T_{TOA} = 61.7$ ms, 153.9 ms, 451.6 ms.

TABLE 1. Correspondence table for the number of samples for the carrier sense N_{CS} and carrier sense parameters assuming actual LPWAN.

N_{CS} carrier sense period (samples)	T_{CS} carrier sense period (ms)	$P_{CS,dBm}$ carrier sense level (dBm)
308	0.77	−119
2547	6.37	−124
23883	59.71	−129
233934	584.84	−134
2323975	5809.94	−139

although good performance can be achieved by centering on $P_{CS,dBm} = -129$ dBm, the performance at the center $P_{CS,dBm} = -129$ dBm slightly deteriorates when compared to the performance at the center.

The difference in the carrier sense period N_{CS} is represented by the multiple solid blue curves in Fig. 9, and this difference corresponds to the difference in the carrier sense level (x-axis) in Fig. 12. Based on this, we have determined the results for the received signal power of the arrived signals to be -119 dBm, which corresponds to the signal-to-noise power ratio (SNR) of approximately -4 dB. This analysis is based on a previous study conducted on the gradient of the characteristics presented in Figs. 9, 10 and 11. Table 1 presents the correspondence table for N_{CS}, T_{CS}, and $P_{CS,dBm}$ under the assumption of an actual LPWAN. The carrier sense levels $P_{CS,dBm} = -119$ dBm, -124 dBm, -129 dBm, -134 dBm -139 dBm correspond to $N_{CS} = 308$, 2547, 23883, 233934, 2323975, respectively, as shown in Table 1.

The results for these N_{CS}s values are presented in Fig. 9. Figs. 10 and 11 depict the performance at approximately -129 dBm in Fig. 12. Additionally, good performance in the signal detection probability can be achieved at the carrier sense levels -119 dBm and -139 dBm, and these performances are superior to the performance achieved at the carrier sense level -129 dBm, as shown in Fig. 12. These results are attributed to the results presented in Fig. 11. Specifically, the theoretical results at $P_{CS,dBm} = -119$ dBm and -139 dBm are the results for high N_{TOA}/N_{CS} and N_{CS}/N_{TOA}, as shown in Fig. 10, and the result obtained at -129 dBm is the result for $N_{TOA}/N_{CS} \approx 1$.

Fig. 13 illustrates the performance of the signal detection probability for $P_{RX,=} - 124$ dBm and $T_{TOA} = 61.7$ ms, 153.9 ms, and 451.6 ms, respectively. Fig. 13 depicts the performances of three types of LoRa signals: $SF = 7$ and 6 byte payload, $SF = 7$ and 50 byte payload, and remaining one is $SF = 10$ and 50 byte payload. The range of good performance widens with the increase in T_{TOA}. This is attributed to the fact that the carrier sense level which satisfies $T_{CS} \approx T_{TOA}$ lowers with the increase in T_{TOA}, and the center of good performance shifts to a low carrier sense level. Furthermore, T_{CS}/T_{TOA} increases with the increase in T_{CS}, which results in a good signal detection probability.

V. NUMERICAL EXAMPLES FOR PERFORMANCE OF ENERGY DETECTION BASED CARRIER SENSE IN LPWAN

A. OVERVIEW

In this section, the performances of LPWAN with the energy detection based carrier sense are numerically analyzed and evaluated based on the results obtained in Sections III and IV.

B. LPWAN MODEL AND PARAMETERS

We consider a simple LPWAN model composed of N_{ED} end devices and one gateway in a communication area with a radius R. All the end devices are randomly deployed in an uniform distribution. LoRaWAN with a single spreading factor is employed as a model of a general LPWAN, and we assume pure ALOHA protocol without acknowledgment as the MAC schemes of LoRaWAN. The general LPWAN is employed to demonstrate the effectiveness of the energy detection based carrier sense without signal orthogonality caused by the difference in the LPWA signals. Each end device transmits its own packet based on a Poisson process at a rate of $1/T_{\mathrm{TX}}$ where T_{TX} is the average transmission period. All the end devices enable retransmission if they cannot transmit their own packet owing to detection by the carrier sense. We let $P_{\mathrm{RX},i}$ denote the received signal power from the ith end device at the gateway, which is given by

$$P_{\mathrm{RX},i} = P_{\mathrm{TX}} - L_i, \tag{29}$$

where P_{TX} and L_i are the transmit power at all end devices and the pass loss between the ith end device and gateway, respectively. L_i can be written as [26],

$$L_i = -10\log_{10}\left(d_i^{\alpha_{\mathrm{GE}}} f_{\mathrm{c}}^2 \times 10^{-2.8}\right), \tag{30}$$

where d_i, α_{GE} and f_{c} are the distance between the ith end device and the gateway, the pass loss exponent between the ith end device and the gateway, and the carrier frequency, respectively. Furthermore, we let $\Theta_{i,k}$ denote the pass loss between the ith and kth end devices, which is given by

$$\Theta_{i,k} = -10\log_{10}\left(\overline{d}_{i,k}^{\alpha_{\mathrm{EE}}} f_{\mathrm{c}}^2 \times 10^{-2.8}\right), \tag{31}$$

where $\overline{d}_{i,k}$ and α_{EE} are the distances between the ith and kth end devices and the pass loss exponent between each end device, respectively. Multiple packets arrive at the gateway if the carrier sense cannot detect signals from other end devices, and the capture effect [27], [28] determines whether packet collision occurs. The capture effect fundamentally indicates that packet with a large received signal power can be received at the gateway. Reference [29] numerically presents that the SNR and signal-to-interference power ratio (SIR) determine the degree of the capture effect. Fig. 14 shows the relationship between the SIR and SNR for LoRa signals with $SF = 7$ and 9, $BW = 200$ kHz and $NF = 6$ dB. The curves shown in Fig. 14 are numerically obtained using computer simulation from the bit error rate characteristics satisfying less than 10^{-5} by changing the SNR and SIR as shown in [29].

TABLE 2. Parameters for numerical examples of LPWAN.

Parameter	Variable	Value
Probability density function of end devices distribution	–	Uniform distributions
Number of end devices	N_{ED}	200
Radius of communication areas	R	$500 \sim 3000$ m
Pass loss exponent (end device - gateway)	α_{GE}	2.7 (suburban)
Pass loss exponent (end device - end device)	α_{EE}	3.3
Transmit power	P_{TX}	13 dBm
Average transmission period (Poisson distribution)	T_{TX}	450 sec
Maximum retransmission times	–	3
Carrier frequency	f_{c}	920 MHz
Noise figure at receiver	NF	6 dB
Number of channels used	–	1

The upper-right area of each curve in Fig. 14 represents the packet transmission success, and the lower-left area of each curve represents the packet collision. The decision of packet collisions based on eq. (21), derived in the previous section, is executed in the numerical simulation to evaluate LPWAN with the energy detection based carrier sense.

Table 2 lists the parameters for the general LPWAN model. The numerical examples presented in the next subsection are executed by changing the radius of the communication area R from 500 to 3000 m, and pass loss exponents are chosen as $\alpha_{\mathrm{GE}} = 2.7$ and $\alpha_{\mathrm{EE}} = 3.3$ assuming the general LPWAN in suburban areas. The transmit power, average transmit period, retransmission time, and carrier frequency of all the end devices are $P_{\mathrm{TX}} = 13$ dBm, $T_{\mathrm{TX}} = 450$ s, 3 times and $f_{\mathrm{c}} = 920$ MHz, respectively. The noise figure at the receiver is 6 dB.

Furthermore, we have assumed that the number of available channels for communication is one. Table 3 lists the three types of LoRa signals employed in the numerical examples. Three types of LoRa signals with different packet length were employed, based on the combination of different spreading factors and payload lengths, as shown in Table 3. Note that each LoRa signal is independently employed for the evaluation owing to the general LPWAN.

C. CHARACTERISTICS OF LPWAN FOR DIFFERENT CARRIER SENSE LEVELS

Fig. 15 presents the packet delivery ratio of the LPWAN with the energy detection based carrier sense. In Fig. 15, $R = 1500$ m is employed, and the three results are compared. The first result is obtained from the evaluation of the LPWAN with the energy detection based carrier sense. The second result is similar to the first result; however, there is no effect of the carrier sense period in the result, that is, a fixed carrier sense period of 128 μs is employed regardless of the carrier sense level. Note that the second result is only presented for the comparison with the first result and is not an evaluation in the actual environment, and furthermore, the carrier sense

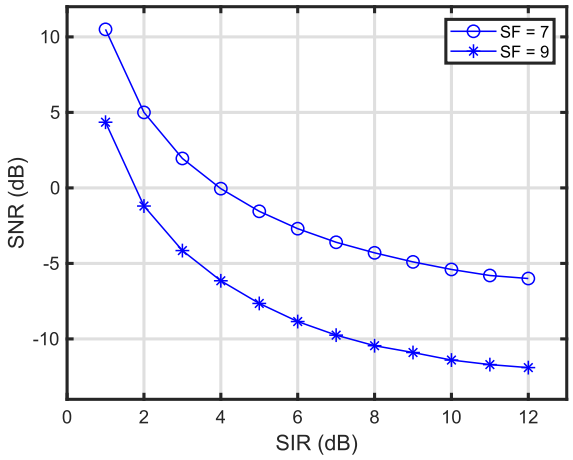

FIGURE 14. Relationship between SIR and SNR for LoRa signals with $SF = 7, 9$, $BW = 200$ kHz and $NF = 6$ dB.

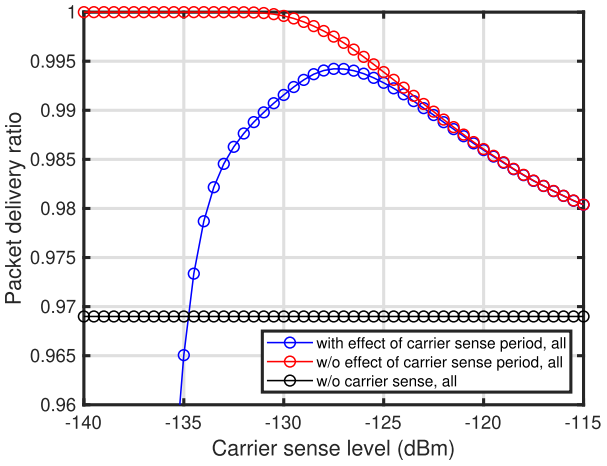

FIGURE 15. Packet delivery ratio for different $P_{\mathrm{CS,dBm}}$. $R = 1500$ m and LoRa signals is "LoRa 1" in Table 3.

TABLE 3. Three types of LoRa signals in numerical examples.

Parameter	Variable	LoRa 1	LoRa 2	LoRa 3
Channel bandwidth (kHz)	BW	200	200	200
Spreading factor	SF	7	7	9
Payload length (byte)	–	6	50	50
Packet length (ms)	T_{TOA}	61.7	153.9	451.6

period 128 μs is regulated in ARIB STD-T108 [6]. The third result is obtained from the evaluation of LPWAN without carrier sense. As shown in Fig. 15, although the performance of the first and second results can be improved as $P_{\mathrm{CS,dBm}}$ decreases, the first result exhibits the best performance at $P_{\mathrm{CS,dBm}} = -127.5$ dBm, whereas the second result approaches a packet delivery ratio of 1. Fig. 3 depicts these characteristics. As shown in Fig. 3, the carrier sense level $P_{\mathrm{CS,dBm}} = -129$ dBm, -134 dBm requires the carrier sense period $T_{\mathrm{CS}} = 59.7$ ms, 584.8 ms, and these T_{CS} values are almost the same or longer than $T_{\mathrm{TOA}} = 61.7$ ms. This results in deterioration in the packet delivery ratio. Fig. 16 depicts the efficiency of carrier sense, which is the probability of detecting a packet even if a collision will not occurred. It can be seen that the probability is approximately 0.67 at $P_{\mathrm{CS,dBm}} = -127.5$ dBm. Furthermore, Fig. 17 presents the packet discard ratio at each end device owing to the limitation of the packet transmission times. The performance of the first result drastically deteriorated to $P_{\mathrm{CS,dBm}}$ below -126 dBm.

We mentioned that too low carrier sense level, that is, too long carrier sense period, deteriorates the accuracy of signal detection in the previous section. However, as shown in these results, even if the carrier sense period is too long, the energy detection based carrier sense can detect the packet, e.g. the RSSI of the packet is relatively higher than the carrier sense level. This may frequently cause a meaningless carrier sense in which the detected packets do not cause a collision, as shown in Fig. 16. As a result, the packet delivery ratio deteriorates. Furthermore, this causes the end devices to lose the opportunity to send packets as shown in Fig. 17.

D. CHARACTERISTICS OF LPWAN FOR DIFFERENT RADII OF COMMUNICATION AREA AND PACKET LENGTH

In this subsection, the relationship between the range of the energy detection based carrier sense and the characteristics of LPWAN. Fig. 18 depicts the packet delivery ratio of the LPWAN with the energy detection based carrier sense for $R = 700$ m, 1000 m, 1500 m, 2000 m, and 3000 m. The packet delivery ratio deteriorates with the increase in the range of the communication area. The carrier sense level at the best performance lowers with the increase in the range of the communication area. The probability that the received signal power from other end devices is less than the carrier sense level, that is, $P_{\mathrm{CS,dBm}} < P_{\mathrm{TX}} - \Theta_{i,k}, \forall i$ at the kth end device demonstrates these characteristics, as shown in Fig. 19. Note that Fig. 19 also represents the evaluation of the effective range of the energy detection based carrier sense, and the arrived signals from all the end devices are more than the carrier sense level for the probability equal to 1. The probability that the arrived signal power from all the end devices is less than the carrier sense level lowers with the increase in the range of the communication area. Furthermore, the results presented in Figs. 18 and 19 demonstrate that the carrier sense level at the best performance of the packet delivery ratio and the probability of $P_{\mathrm{CS,dBm}} < P_{\mathrm{TX}} - \Theta_{i,k}, \forall i$ being equal to 1 are almost identical. However, both the carrier sense levels do not concur as the radius of the communication area increases. Although the detectable end devices increase by lowering the carrier sense level, the effect of the meaningless carrier sense owing to the decrease in the carrier sense level outweighs this, and the performance of the LPWAN cannot be improved at some carrier sense levels. This also indicates that none of the end devices in the communication area can be detected, even at an optimal carrier sense level; thus, it can be

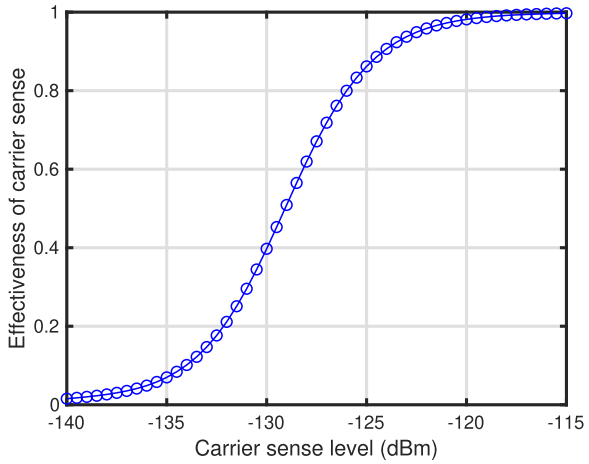

FIGURE 16. Efficiency of carrier sense for different $P_{\mathrm{CS,dBm}}$. $R = 1500$ m and LoRa signals is "LoRa 1" in Table 3.

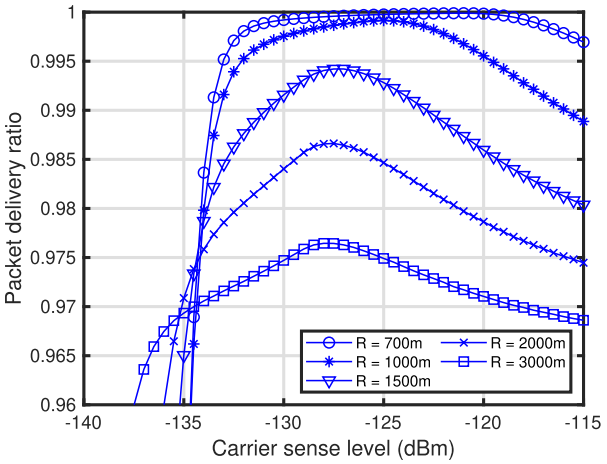

FIGURE 18. Packet delivery ratio for different $P_{\mathrm{CS,dBm}}$. $R = 700$ m, 1000 m, 1500 m, 2000 m, 3000 m and LoRa signals is "LoRa 1" in Table 3.

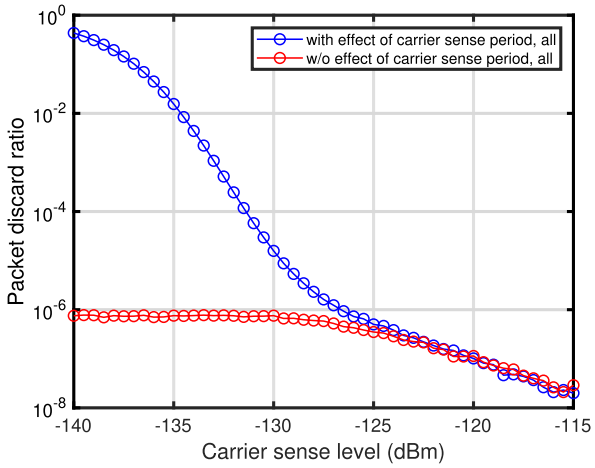

FIGURE 17. Packet discard ratio for different $P_{\mathrm{CS,dBm}}$. $R = 1500$ m and LoRa signals is "LoRa 1" in Table 3.

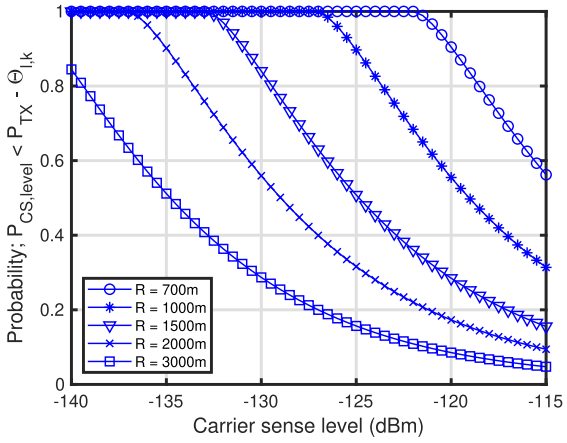

FIGURE 19. Probability that $P_{\mathrm{CS,dBm}} < P_{\mathrm{RX}} - \Theta_{i,k}, \forall i$ at kth end device for different $P_{\mathrm{CS,dBm}}$. $R = 700$ m, 1000 m, 1500 m, 2000 m, 3000 m and LoRa signals is "LoRa 1" in Table 3.

considered to be the performance limit of the energy detection based carrier sense.

The carrier sense levels which can achieve the results for the ratio $T_{\mathrm{TOA}}/T_{\mathrm{CS}}$ are presented in Fig. 21 for the best performances of the packet delivery ratio for each R, as shown in Fig. 18. In Fig. 21, the performances of the three LoRa signals listed in Table 3 are shown. The optimum carrier sense level lowers with the increase in T_{TOA} or R. The longer the packet length on air around the end devices, the higher the $T_{\mathrm{TOA}}/T_{\mathrm{CS}}$. Consequently, the optimum carrier sense level becomes low. In addition, the optimal carrier sense level decreases by 2 dB as T_{TOA} increases by approximately 3 times. Fig. 21 shows that the $T_{\mathrm{CS}}/T_{\mathrm{TOA}}$ in Fig. 20. $T_{\mathrm{TOA}}/T_{\mathrm{CS}}$ lowers with the increase in R, and all the results presented in Fig. 20 converge to $T_{\mathrm{TOA}}/T_{\mathrm{CS}} \approx 2$, as R increases.

E. EFFECT OF NOISE POWER ESTIMATION ACCURACY ON PERFORMANCE OF LPWAN

In this subsection, we discuss the effect of noise power estimation accuracy on the performance of LPWAN. First, we evaluate the effect caused by thermal changes on the performance. To evaluate the effect, we employ the minimum SNR for energy detection based on the estimated noise power (eq. (34) in [25]), as shown in the following equation,

$$SNR_{\mathrm{min,ED}} \approx \frac{1 + \mathcal{Q}^{-1}\left(\overline{P_{\mathrm{FA}}}\right)\sqrt{\frac{N_{\mathrm{CS}}+N_{\mathrm{EST}}}{N_{\mathrm{CS}}N_{\mathrm{EST}}}}}{1 + \mathcal{Q}^{-1}\left(\overline{P_{\mathrm{D}}}\right)\sqrt{\frac{N_{\mathrm{CS}}+N_{\mathrm{EST}}}{N_{\mathrm{CS}}N_{\mathrm{EST}}}}} - 1, \tag{32}$$

where N_{EST} is the number of samples for noise power estimation. Based on eq. (32) and the noise power, achievable carrier sense level $\overline{P_{\mathrm{CS,dBm}}}$ can be obtained as,

$$\overline{P_{\mathrm{CS,dBm}}} \approx SNR_{\mathrm{min,ED}} - 174 + 10\log_{10}(BW) + NF. \tag{33}$$

Note that the noise power η_{dBm} for given $BW = 200$ kHz and $NF = 6$ dB is $\eta_{\mathrm{dBm}} \approx -115$ dBm. Fig. 22 shows the achievable carrier sense level for $N_{\mathrm{EST}} = \sqrt{N_{\mathrm{EST}}}, N_{\mathrm{CS}}, N_{\mathrm{CS}}^{1.5}$. As shown in Fig. 22, the carrier sense level lower the noise power can be achieved for the $N_{\mathrm{EST}} = N_{\mathrm{CS}}^{1.5}$ case. Furthermore, the carrier sense level can be approximately achieved for the $N_{\mathrm{EST}} = N_{\mathrm{CS}}$ case.

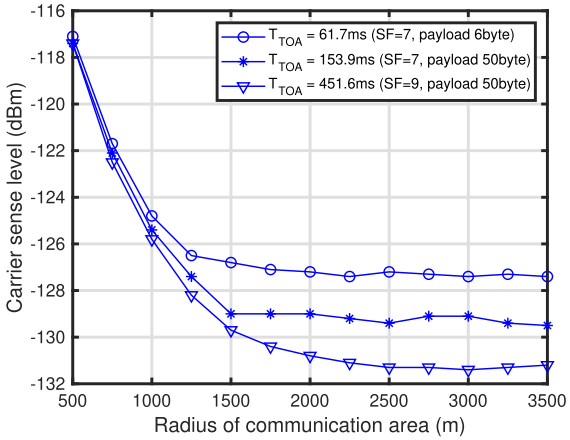

FIGURE 20. Relationship between radius of communication area and optimal carrier sense level for three types of LoRa signals listed in Table 3.

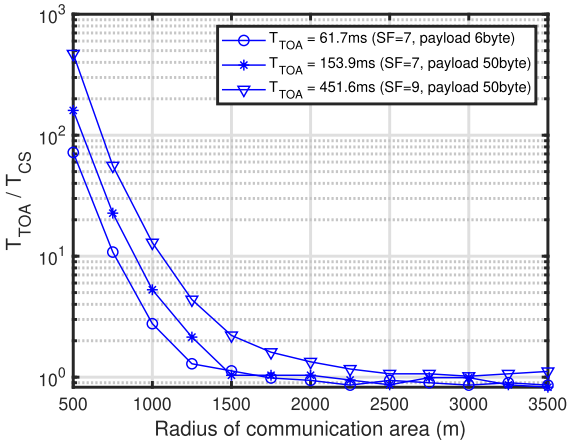

FIGURE 21. Relationship between radius of communication area and T_{TOA}/T_{CS} for three types of LoRa signals listed in Table 3.

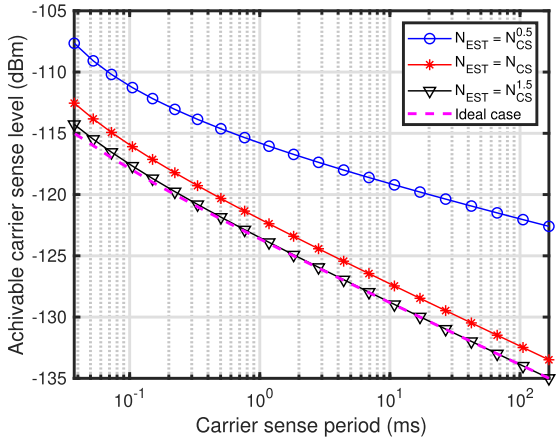

FIGURE 22. Achievable carrier sense level for different carrier sense periods and N_{EST}.

However, there are interferences during the period for noise power estimation, and they also causes the inaccurate estimation result [25]. For example, to avoid the degradation of the estimation results caused by interferences, quiet periods, which are synchronized among the secondary users,

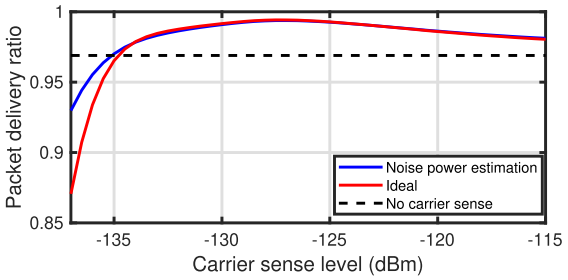

(a) $N_{ED} = 200$ and $N_I = 0$

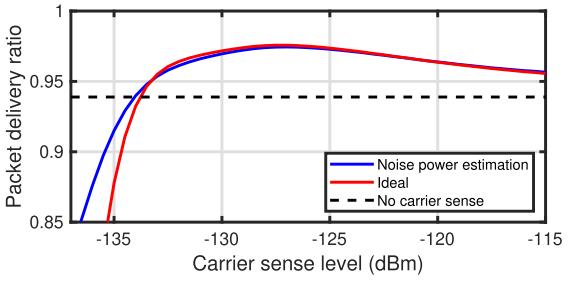

(b) $N_{ED} = 200$ and $N_I = 200$

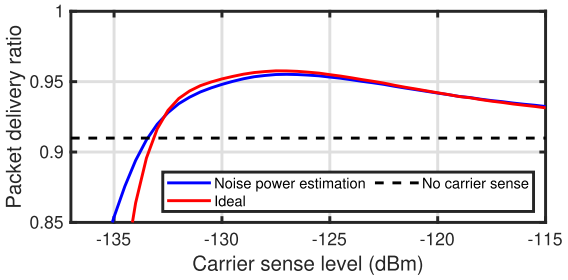

(c) $N_{ED} = 200$ and $N_I = 400$

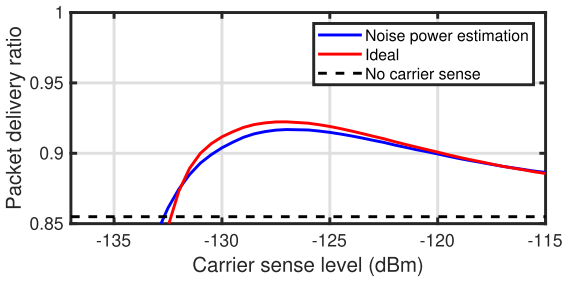

(d) $N_{ED} = 200$ and $N_I = 800$

FIGURE 23. Packet delivery ratio in LPWAN based on energy detection based carrier sense with noise power estimation. Performances shown in the figure are evaluated in environment where there are interference end devices without the carrier sense from other LPWANs arrives. $N_{ED} = 200$ and $N_I = 0, 200, 400, 800$.

are employed in the standards IEEE 802.22 [30]. However, it is difficult to employ quiet period at LPWAN where there are interferences in the same frequency band because it is possible to build a private network. Therefore, we reveal the effect of interferences on the performance of LPWAN with the energy detection based carrier sense using computer simulation under the same LPWA parameters as in Table 2. Furthermore, we employ "LoRa 1" listed in Table 3 as LPWA signal. Each end device estimates the noise power one second before the carrier sense, using a period of the same length as

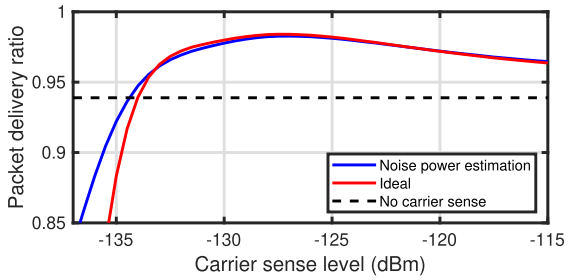

(a) $N_{\mathrm{ED}} = 200$ and $N_{\mathrm{I}} = 200$

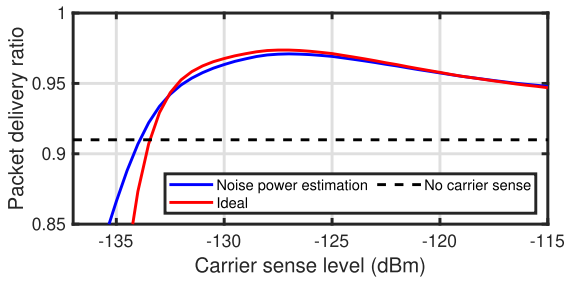

(b) $N_{\mathrm{ED}} = 200$ and $N_{\mathrm{I}} = 400$

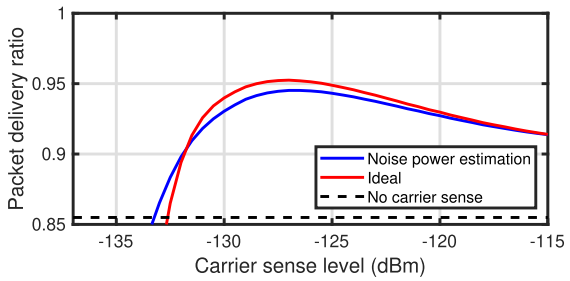

(c) $N_{\mathrm{ED}} = 200$ and $N_{\mathrm{I}} = 800$

FIGURE 24. Packet delivery ratio in LPWAN based on energy detection based carrier sense with noise power estimation. Performances shown in the figure are evaluated in environment where there are interference end devices with the carrier sense ($P_{\mathrm{CS,dBm}} = -120$ dBm) from other LPWANs arrives. $N_{\mathrm{ED}} = 200$ and $N_{\mathrm{I}} = 200, 400, 800$.

the carrier sense period. The estimated noise power is used to the threshold for the carrier sense the immediately follows. The estimated noise power $\widetilde{\sigma}_v^2$ is given by,

$$\widetilde{\sigma}_v^2 = \sigma_v^2 + \Delta\sigma_v^2 + \sigma_{\mathrm{I}}^2. \tag{34}$$

where $\Delta\sigma_v^2$ is the component of inaccurate estimation resulting from taking the average of a finite length sample and $\Delta\sigma_v^2 \sim \mathcal{N}\left(0, \sigma_v^4/N_{\mathrm{CS}}\right)$. σ_{I}^2 is the arrival interference power during the noise power estimation at the end device. Note that σ_{I}^2 is equal to zero if there are no arrival interferences during the noise power estimation. Furthermore, we employ N_{I} interference end devices that are not included in the N_{ED} end devices. The parameters for the interference end devices are basically the same as in Table 2, and we employ "LoRa 1" listed in Table 3 as the interference signal. Fig. 23 shows the performance of the packet delivery ratio in the LPWAN employing the energy detection based carrier sense with the noise power estimation. In Fig. 23, the performances of the LPWAN consisting of $N_{\mathrm{ED}} = 200$ end devices in the case, where their $N_{\mathrm{I}} = 0, 200, 400, 800$ end devices do not execute the energy detection based carrier sense, is evaluated. As shown in Fig. 23, although the arrival interferences during the estimation certainly degrades the packet delivery ratio as N_{I} increases, its performance outperforms the case without the carrier sense. Therefore, it can be said that the effect of interference avoidance by the energy detection based carrier sense outweigh the effect of the degradation of the noise power estimation accuracy owing to the interferences. Furthermore, we evaluate the performances of the LPWAN in the case where their $N_{\mathrm{I}} = 200, 400, 800$ end devices execute the energy detection based carrier sense with $P_{\mathrm{CS,dBm}} = -120$ dBm. It can be seen that the effect of the interference avoidance is more effective compare to Fig. 23. The fact also indicates that the energy detection based carrier sense is valid to avoid the interferences from other LPWANs in the vicinity of own network.

VI. CONCLUSION

This paper presented the detailed discussion on the performance of the energy detection based carrier sense in the LPWAN in order to detect the target signal with the power lower than the noise power and employ it in the wide communication area. We theoretically derived two new factors as the signal detection deterioration factors, in addition to the factors reported so far. The new factors are the arbitrary start time of the carrier sense for the arrived signal and the finite ratio $T_{\mathrm{TOA}}/T_{\mathrm{CS}}$. Furthermore, the performance of LPWAN with the energy detection based carrier sense was numerically verified based on these theoretical analyses. The numerical examples demonstrate that the energy detection based carrier sense improves the performance of the LPWAN. Furthermore, the numerical examples indicated that a carrier sense level that is too low produces the meaningless carrier sense and packet discard at the end device, and this results in drastic deterioration of the performance of the LPWAN. Therefore, the carrier sense period should be determined by packet length in the networks. Furthermore, based on the references [23], [24], and [25], the performances of LPWAN with the inaccurate noise power estimation were evaluated. In the evaluation, we showed that the effect of interference avoidance by the energy detection based carrier sense outweigh the effect of the degradation of the noise power estimation accuracy owing to the interferences.

The future work involves the development of a design method for the energy detection based carrier sense considering the packet length on air around the end devices, the energy consumption of the end devices, and the radiowave propagation environment, such as a shadowing component between each end device.

REFERENCES

[1] U. Raza, P. Kulkarni, and M. Sooriyabandara, "Low power wide area networks: An overview," *IEEE Commun. Surveys Tuts.*, vol. 19, no. 2, pp. 855–873, 2nd Quart., 2017.
[2] *LoRa Alliance*. Accessed: Mar. 17, 2022. [Online]. Available: https://lora-alliance.org/
[3] *LoRa Modulation Basics-AN1200.22, Rev. 2.*, Semtech Corporat., Camarillo, CA, USA, 2015.

[4] P. Beecher, "Comparing IoT networks at a glance," Wi-SUN Alliance, San Ramon, CA, USA, White Paper, Dec. 2017. Accessed: May 28, 2021. [Online]. Available: https://www.wi-sun.org/wp-content/uploads/WiSUN-Alliance-Comparing_IoT_Networks-r1.pdf
[5] *Sigfox—The Global Communication Service Provider for the Internet of Things (IoT)*. Accessed: Mar. 17, 2022. [Online]. Available: https://www.sigfox.com/en
[6] *ARIB STD-T108*, V.1.2, Assoc. Radio Ind. Bus., Jan. 2018.
[7] L. Kleinrock and F. Tobagi, "Packet switching in radio channels: Part I—Carrier sense multiple-access modes and their throughput-delay characteristics," *IEEE Trans. Commun.*, vol. C-23, no. 12, pp. 1400–1416, Dec. 1975.
[8] *RP002-1.0.0 LoRaWAN Regional Parameters*, LoRa Alliance Tech. Committee, Nov. 2019.
[9] S. M. Kay, *Fundamentals of Statistical Signal Processing: Detection Theory*. Upper Saddle River, NJ, USA: Prentice-Hall, 1998.
[10] H. Urkowitz, "Energy detection of unknown deterministic signals," *Proc. IEEE*, vol. 55, no. 4, pp. 523–531, Apr. 1967.
[11] R. Tandra and A. Sahai, "Fundamental limits on detection in low SNR under noise uncertainty," in *Proc. Int. Conf. Wireless Netw., Commun. Mobile Comput.*, 2005, pp. 464–469.
[12] W. A. Gardner, "Exploitation of spectral redundancy in cyclostationary signals," *IEEE Signal Process. Mag.*, vol. 8, no. 2, pp. 14–36, Apr. 1991.
[13] *SX1272 | Long Range, Low Power RF Transceiver 860-1000MHz | Semtech*. Accessed: Mar. 17, 2022. [Online]. Available: https://www.semtech.com/products/wireless-RF/lora-transceivers/sx1272
[14] T. H. Kim, J. Ni, R. Srikant, and N. H. Vaidya, "Throughput-optimal CSMA with imperfect carrier sensing," *IEEE/ACM Trans. Netw.*, vol. 21, no. 5, pp. 1636–1650, Oct. 2013.
[15] I. Ramachandran and S. Roy, "Analysis of throughput and energy efficiency of p-persistent CSMA with imperfect carrier sensing," in *Proc. GLOBECOM. IEEE Global Telecommun. Conf.*, Feb. 2005.
[16] S. G. Glisic, "1-persistent carrier sense multiple access in radio channels with imperfect carrier sensing," *IEEE Trans. Commun.*, vol. 39, no. 3, pp. 458–464, Mar. 1991.
[17] J. Ortín, M. Cesana, and A. Redondi, "Augmenting LoRaWAN performance with listen before talk," *IEEE Trans. Wireless Commun.*, vol. 18, no. 6, pp. 3113–3128, Jun. 2019.
[18] T.-H. To and A. Duda, "Simulation of LoRa in NS-3: Improving LoRa performance with CSMA," in *Proc. IEEE Int. Conf. Commun. (ICC)*, May 2018, pp. 1–7.
[19] L. Beltramelli, A. Mahmood, P. Österberg, and M. Gidlund, "LoRa beyond ALOHA: An investigation of alternative random access protocols," *IEEE Trans. Ind. Informat.*, vol. 17, no. 5, pp. 3544–3554, May 2021.
[20] B. Razavi, *RF Microelectronics*, 2nd ed. Upper Saddle River, NJ, USA: Prentice-Hall, 2012.
[21] A. Papoulis, *Random Variables and Stochastic Processes*, 4th ed. New York, NY, USA: McGraw-Hill, 2002.
[22] J. G. Proakis, *Digital Communications*, 4th ed. New York, NY, USA: McGraw-Hill, 2001.
[23] R. Tandra and A. Sahai, "SNR walls for signal detection," *IEEE J. Sel. Topics Signal Process.*, vol. 2, no. 1, pp. 4–17, Feb. 2008.
[24] S. Shellhammer et al., *Spectrum Sensing Requirements Summary*, IEEE Standard 802.22-06/0089r5, Sep. 2006.
[25] A. Mariani, A. Giorgetti, and M. Chiani, "Effects of noise power estimation on energy detection for cognitive radio applications," *IEEE Trans. Commun.*, vol. 59, no. 12, pp. 3410–3420, Dec. 2011.
[26] A. Waret, M. Kaneko, A. Guitton, and N. El Rachkidy, "LoRa throughput analysis with imperfect spreading factor orthogonality," *IEEE Wireless Commun. Lett.*, vol. 8, no. 2, pp. 408–411, Apr. 2019.
[27] J. Arnbak and W. van Blitterswijk, "Capacity of slotted ALOHA in Rayleigh-fading channels," *IEEE J. Sel. Areas Commun.*, vol. JSAC-5, no. 2, pp. 261–269, Feb. 1987.
[28] A. U. H. Sheikh, Y.-D. Yao, and X. Wu, "The ALOHA systems in shadowed mobile radio channels with slow or fast fading," *IEEE Trans. Veh. Technol.*, vol. 39, no. 4, pp. 289–298, Nov. 1990.
[29] T. Elshabrawy and J. Robert, "Capacity planning of LoRa networks with joint noise-limited and interference-limited coverage considerations," *IEEE Sensors J.*, vol. 19, no. 11, pp. 4340–4348, Jun. 2019.
[30] C. Cordeiro, K. Challapali, D. Birru, and S. Shankar, "IEEE 802.22: The first worldwide wireless standard based on cognitive radios," in *Proc. 1st IEEE Int. Symp. New Frontiers Dyn. Spectr. Access Netw.*, Nov. 2005, pp. 328–337.

SHUSUKE NARIEDA (Member, IEEE) received the B.E. and M.E. degrees from the University of the Ryukyus, in 1999 and 2001, respectively, and the Ph.D. degree from Osaka Prefecture University, in 2006. Since 2001, he has been with Johokobo Inc., as a Software Development Engineer. Since 2006, he has been with Yazaki Corporation as a Research and Development Engineer. Since 2009, he has been an Associate Professor with the Department of Electrical and Computer Engineering, National Institute of Technology, Akashi College, Japan. Currently, he is an Associate Professor with the Graduate School of Engineering, Mie University, Japan. His current research interests include distributed signal processing for wireless sensor networks and spectrum sensing techniques for cognitive radio networks, hardware and system design for high-performance wireless communication systems, and general signal processing and communication theories. He is a member of the IEICE of Japan. He received the Best Paper Award at the 2015 IEEE CORAL and the Best Paper Award at the 2023 ICOIN.

TAKEO FUJII (Senior Member, IEEE) received the B.E., M.E., and Ph.D. degrees in electrical engineering from Keio University, Yokohama, Japan, in 1997, 1999, and 2002, respectively. From 2000 to 2002, he was a Research Associate with the Department of Information and Computer Science, Keio University. From 2002 to 2006, he was an Assistant Professor with the Department of Electrical and Electronic Engineering, Tokyo University of Agriculture and Technology. From 2006 to 2014, he was an Associate Professor with the Advanced Wireless Communication Research Center, The University of Electro-Communications, where he is currently a Professor and the Director. His current research interests include cognitive radio and ad-hoc wireless networks. He received the Best Paper Award in the Fall 1999 IEEE VTC, the 2001 Active Research Award in Radio Communication Systems from the IEICE Technical Committee of RCS, the 2001 Ericsson Young Scientist Award, the Young Researcher's Award from IEICE, in 2004, the Young Researcher Study Encouragement Award from the IEICE Technical Committee of AN, in 2009, the Best Paper Award in the 2013 IEEE CCNC, and the IEICE Communication Society Best Paper Award, in 2016.